Proteasome assembly defect due to a proteasome subunit beta type 8 (PSMB8) mutation causes the autoinflammatory disorder, Nakajo-Nishimura syndrome

Kazuhiko Arima[a,1], Akira Kinoshita[b,1], Hiroyuki Mishima[b,1], Nobuo Kanazawa[c,1], Takeumi Kaneko[d], Tsunehiro Mizushima[e], Kunihiro Ichinose[a], Hideki Nakamura[a], Akira Tsujino[f], Atsushi Kawakami[a], Masahiro Matsunaka[c], Shimpei Kasagi[g], Seiji Kawano[g], Shunichi Kumagai[g], Koichiro Ohmura[h], Tsuneyo Mimori[h], Makito Hirano[i], Satoshi Ueno[i], Keiko Tanaka[j], Masami Tanaka[k], Itaru Toyoshima[l], Hirotoshi Sugino[m], Akio Yamakawa[n], Keiji Tanaka[o], Norio Niikawa[p], Fukumi Furukawa[c], Shigeo Murata[d], Katsumi Eguchi[a], Hiroaki Ida[a,q,2], and Koh-ichiro Yoshiura[b,2]

[a]Unit of Translational Medicine, Department of Immunology and Rheumatology, Graduate School of Biomedical Sciences, Nagasaki University, Nagasaki 852-8501, Japan; [b]Department of Human Genetics, Graduate School of Biomedical Sciences, Nagasaki University, Nagasaki 852-8523, Japan; [c]Department of Dermatology, Wakayama Medical University, Wakayama 641-0012, Japan; [d]Laboratory of Protein Metabolism, Graduate School of Pharmaceutical Sciences, The University of Tokyo, Bunkyo-ku, Tokyo 113-0033, Japan; [e]Department of Life Science, Picobiology Institute, Graduate School of Life Science, University of Hyogo, Kamigori-cho, Ako-gun, Hyogo 678-1297, Japan; [f]Unit of Translational Medicine, Department of Neuroscience and Neurology, Nagasaki University Graduate School of Biomedical Sciences, Nagasaki 852-8501; [g]Department of Clinical Pathology and Immunology, Kobe University Graduate School of Medicine, Kobe 650-0017, Japan; [h]Department of Rheumatology and Clinical Immunology, Graduate School of Medicine, Kyoto University, Kyoto 606-8507, Japan; [i]Department of Neurology, Nara Medical University, Kashihara, Nara 634-8522, Japan; [j]Department of Neurology, Kanazawa Medical University, Kahoku-gun, Ishikawa 920-0293, Japan; [k]Department of Neurology, Utano National Hospital, Ukyou-ku, Kyoto 616-8255, Japan; [l]Department of Neurology and Medical Education Center, Akita University School of Medicine, Akita 010-8543, Japan; [m]Sugino Pediatric Clinic, Asakita-ku, Hiroshima 731-0231, Japan; [n]Office of Strategic Management, Institute of Medical Science, The University of Tokyo, Minato-ku, Tokyo 108-8639, Japan; [o]Laboratory of Protein Metabolism, Tokyo Metropolitan Institute of Medical Science, Setagaya-ku, Tokyo 156-8506, Japan; [p]Research Institute of Personalized Health Sciences, Health Sciences University of Hokkaido, Ishikari-Tobetsu, Hokkaido 061-0293, Japan; and [q]Division of Respirology, Neurology, and Rheumatology, Department of Medicine, Kurume University School of Medicine, Kurume, Fukuoka 830-0011, Japan

Edited* by Daniel Kastner, National Institutes of Health, Bethesda, MD, and approved July 21, 2011 (received for review April 14, 2011)

Nakajo-Nishimura syndrome (NNS) is a disorder that segregates in an autosomal recessive fashion. Symptoms include periodic fever, skin rash, partial lipomuscular atrophy, and joint contracture. Here, we report a mutation in the human proteasome subunit beta type 8 gene (PSMB8) that encodes the immunoproteasome subunit β5i in patients with NNS. This G201V mutation disrupts the β-sheet structure, protrudes from the loop that interfaces with the β4 subunit, and is in close proximity to the catalytic threonine residue. The β5i mutant is not efficiently incorporated during immunoproteasome biogenesis, resulting in reduced proteasome activity and accumulation of ubiquitinated and oxidized proteins within cells expressing immunoproteasomes. As a result, the level of interleukin (IL)-6 and IFN-γ inducible protein (IP)-10 in patient sera is markedly increased. Nuclear phosphorylated p38 and the secretion of IL-6 are increased in patient cells both in vitro and in vivo, which may account for the inflammatory response and periodic fever observed in these patients. These results show that a mutation within a proteasome subunit is the direct cause of a human disease and suggest that decreased proteasome activity can cause inflammation.

Nakajo-Nishimura syndrome (NNS) (MIM256040, ORPHA-2615) is a distinct inflammatory and wasting disease. It was first reported by Nakajo in 1939, followed by Nishimura in 1950, and was called "secondary hypertrophic osteoperiostosis with pernio" (1, 2). More than 20 cases of this disease have been reported in various clinical fields, all from Japan (3–8). The disease was soon recognized as a new entity and was called "a syndrome with nodular erythema, elongated and thickened fingers, and emaciation" or "hereditary lipomuscular atrophy with joint contracture, skin eruptions and hyper-γ-globulinemia" on the basis of the common characteristic features (3, 4).

NNS usually begins in early infancy with a pernio-like rash. The patient develops periodic high fever, nodular erythema-like eruptions, and myositis. Lipomuscular atrophy and joint contractures gradually progress, mainly in the upper body, to form the characteristic thin facial appearance and elongated clubbed fingers. Inflammatory changes are marked and include constantly elevated erythrocyte sedimentation rate (ESR) and C-reactive protein (CRP), hyper-γ-globulinemia, hepatosplenomegaly, basal ganglia calcification, and focal mononuclear cell infiltration with vasculopathy on histopathology. Autoantibodies are negative at the onset of NNS; although, in some cases, titers increase as the disease progresses.

Although NNS bears similarities to other autoimmune diseases, particularly dermatomyositis, it is only in recent years that its similarity to autoinflammatory periodic fever syndromes has been pointed out (5, 6). Oral steroids are effective in treating the inflammation, but not the wasting, and most patients die as a result of respiratory or cardiac failure. Despite the predicted segregation in an autosomal recessive fashion, the gene responsible has not been identified. Here, we describe a mutation in the human *PSMB8* that encodes the immunoproteasome subunit β5i in NNS patients.

Proteasomes collaborate with the ubiquitin system, which tags proteins with a polyubiquitin chain and marks them for degradation. The 26S proteasome is a multisubunit protease responsible for regulating proteolysis in eukaryotic cells in collaboration with the ubiquitin system. This ubiquitin–proteasome system is involved in various biological processes, including immune responses, DNA repair, cell cycle progression, transcription and protein quality control. It comprises a single catalytic 20S proteasome with 19S regulatory particles (RPs) attached to the ends (9–11). The 20S proteasome comprises 28 subunits arranged as a cylindrical particle containing four heteroheptameric rings: $\alpha_{1-7}\beta_{1-7}\beta_{1-7}\alpha_{1-7}$. Only three of the β subunits, β1, β2, and β5, are proteolytically active in the standard 20S pro-

Author contributions: N.K., A.Y., N.N., F.F., S.M., K.E., H.I., and K.-i.Y. designed research; K.A., A. Kinoshita, H.M., N.K., T.K., T. Mizushima, K.I., H.N., A.T., A. Kawakami, M.M., S. Kasagi, S. Kawano, S. Kumagai, K.O., T. Mimori, M.H., S.U., Keiko Tanaka, M.T., I.T., H.S., S.M., H.I., and K.-i.Y. performed research; K.A., A. Kinoshita, H.M., N.K., A.Y., S.M., H.I., and K.-i.Y. analyzed data; and N.K., Keiji Tanaka, F.F., S.M., H.I., and K.-i.Y. wrote the paper.

The authors declare no conflict of interest.

*This Direct Submission article had a prearranged editor.

[1]K.A., A. Kinoshita, H.M., and N.K. contributed equally to this work.

[2]To whom correspondence may be addressed. E-mail: kyoshi@nagasaki-u.ac.jp or ida@med.kurume-u.ac.jp.

This article contains supporting information online at www.pnas.org/lookup/suppl/doi:10.1073/pnas.1106015108/-/DCSupplemental.

teasome. Each of the three β subunits preferentially cleaves an acidic, basic, or hydrophobic residue, activities often referred to as caspase-like, trypsin-like, or chymotrypsin-like, respectively.

In vertebrates, there are three additional IFN-γ–induced subunits: β1i, β2i, and β5i. These are preferentially incorporated into the 20S proteasome in place of the standard subunits to form the immunoproteasome in immune cells such as macrophages, T and B cells, and dendritic cells, whereas their expression is low in nonlymphoid peripheral tissues. This results in more efficient production of MHC class I epitopes (12). The present study analyzed the activity of proteasomes with a mutated β5i subunit, and the subsequent inflammatory signal transduction pathways in mutant cells. The results suggest that the *PSMB8* mutation evokes an inflammatory response in humans, and that the p38 pathway may play an important role in inflammation in NNS patients.

Recently, a different mutation in the *PSMB8* gene was reported in patients with a disease similar to, but distinct from, NNS: an autosomal recessive syndrome of joint contracture, muscular atrophy, microcytic anemia, and panniculitis-associated lipodystrophy (JMP) (13, 14). The mutation in JMP syndrome, T75M, causes a reduction in chymotrypsin-like activity only, without disrupting the activity of other peptidases (13). In contrast, the G201V mutation identified in NNS patients results in the loss of all peptidase activity because of assembly defects and reduced proteasome levels. Thus, the discovery of *PSMB8* mutations in these related diseases indicates the presence of a distinct class of proteasome-associated autoinflammatory disorders.

Results

Clinical Features of NNS Patients. National surveillance in Japan confirms that only around 10 NNS patients are alive today. Therefore, preserved fibroblasts from an autopsy case (patient 1) were provided for genetic analysis, following approval by the local ethical committee. Of the living cases, written informed consent to undertake genetic and molecular analyses was obtained from six patients. The clinical features of all seven cases are summarized in Table S1. Patients 1, 2, and 4 were born to consanguineous parents and their clinical features have been described previously (Fig. S1*A*) (6, 8). The other patients are sporadic cases collected for this study and were born in the limited area between south Osaka and Wakayama. A diagnosis of NNS is not difficult owing to the characteristic features, including the thin facial appearance and long clubbed fingers (Fig. S1*B*). The clinical course throughout childhood was variable: from no medical consultation in the case of patient 7, to administration of oral steroids since infancy in patients 3 and 6. Partial lipomuscular atrophy with long clubbed fingers plus a pernio-like, heliotrope-like, or nodular erythema-like skin rash were observed in all cases, and periodic fever and joint contractures in most but not all. Wheras hyperhidrosis was also observed in some cases, short stature and low IQ were seen only in patients 6 and 1, respectively. Indeed, patient 6 was treated with growth hormone, although growth retardation in this case may have been due, in part, to oral steroids. Chronic inflammation, indicated by elevated ESR and hyper-γ-globulinemia, were observed in all patients, and microcytic anemia, high serum creatine phosphokinase (CPK), hepatosplenomegaly, and basal ganglia calcification were present in most, but not all. Notably, various autoantibodies (with a mildly elevated titer of antinuclear antibodies) were detected in half of the patients. The most striking differences between NNS and JMP are the absence of fever in JMP syndrome and the absence of seizures in NNS (14) (Table S1).

Genetic Mapping and Mutation Searches. We examined genomic DNA samples from five patients (patients 1–5) and three unaffected siblings of patient 4 using an Affymetrix GeneChip Human Mapping 500K array set (Nsp I and Sty I arrays), and the BRLMM genotyping algorithm. Because the runs of homozygosity (ROHs) shared by all patients were expected to be candidate regions containing the gene responsible for the disease, we identified a region spanning 1.1 Mb on chromosome 6p21.31–32 [from 32,798,004–33,903,106; National Center for Biotechnology Information (NCBI) build 36.1] as the sole candidate region responsible for NNS (Fig. 1*A*). We directly sequenced 436 coding exons in the 44 genes within this candidate region, including the splicing sites. A single nonsynonymous variation (not registered in the dbSNP database) was identified in exon 5 of *PSMB8* (NM_148919 in the NCBI database), designated *LMP7* or *RING10*, which encodes the LMP7 protein (β5i subunit) of the immunoproteasome. This mutation was a guanine to thymine transversion at nucleotide position 602 (c.602G > T) (Fig. 1*B*). Haplotype analysis indicated that the G201V mutation was probably introduced into the Japanese population by a single founder, as the haplotype around this mutation was identified in all patients (Fig. S1*C*). Gly201, which is a highly conserved residue in the β5i subunit (Fig. 1*C*) and among mature proteasome subunits in vertebrates (Fig. S1*D*), is substituted by Val (G201V) (Fig. 1*B*).

Impaired Immunoproteasome Assembly and Peptidase Activity. In silico modeling of the mutant β5i ($\beta5i^{G201V}$) subunit was used to infer the conformational impact of this mutation because the assembly of the proteasome is a highly orchestrated and complex process (9, 15). The β5i subunit is cleaved between amino acid residues Gly72 and Thr73 to yield the active form (16), in which the catalytic center is generated by Thr73, Asp89, Arg91, and Lys105. The mutated residue at position 201 was located at the edge of the S8 β-sheet of β5i and was close to its catalytic threonine residue Thr73 (Fig. 2*A*). The G201V substitution caused conformational changes not only in Thr73 but also in Lys105 within the catalytic center (Fig. S2). The mutation resulted in further conformational changes in the S8–H3 loop located at the

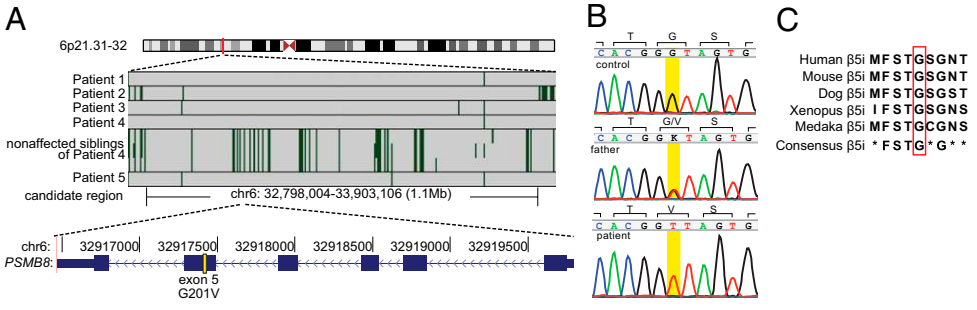

Fig. 1. SNP microarray-based homozygosity mapping and mutation search. (*A*) Homozygosity mapping for NNS patients and nonaffected siblings. ROH regions were detected using a hidden Markov model-based algorithm. The sole candidate region identified within 6p21.31–32 is shown. Green vertical lines indicate heterozygous SNPs and the background gray area indicates a region without heterozygous SNP calls. To be conservative, we did not regard isolated single heterozygous calls as delimiting ROH regions. The physical positions are shown in NCBI build 36.1. Patient numbers correspond to Figs. S1*A* and S1*C* and Table S1. No history of consanguineous marriage was apparent for patients 3 and 5, according to the family history interview. (*B*) Chromatograms for a control, a patient's father, and a patient. A mutation in *PSMB8* exon 5 identified in NNS patients by sequencing is highlighted in yellow. (*C*) Amino acid comparisons with other species. The glycine at the mutation site (red box) is highly conserved among vertebrates.

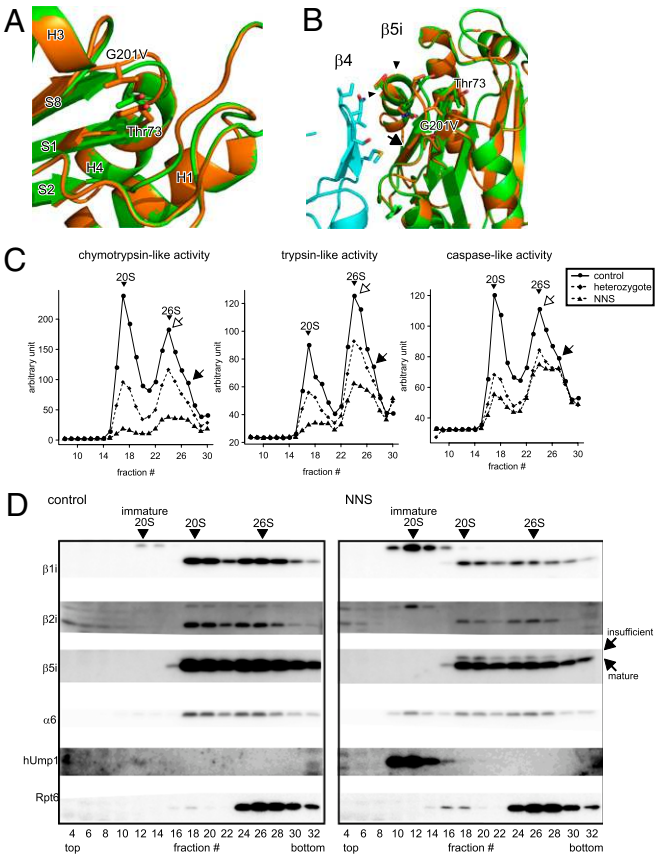

Fig. 2. G201V mutation in β5i reduces proteasome activity in immunoproteasome-expressing cells. (*A*) Close-up view of the mutation site (G201V) within β5i. Structural models of G201V β5i (orange) and wild-type β5i (green) were created from the β5-subunit structure [Protein Data Bank (PDB) ID code 1IRU]. The secondary structure elements for β5i are labeled. Val201 and Thr73 are shown in the stick model. Thr73 is a catalytic residue of β5i. (*B*) A ribbon diagram of the β4–β5i complex. The arrow shows the difference in the β-sheet between β5i (green) and $β5i^{G201V}$ (orange). Arrowheads show the protruding S8–H3 loop of $β5i^{G201V}$. (*C*) Peptidase activity of LCLs. Extracts were fractionated by glycerol gradient centrifugation (8–32% glycerol from fraction 1–32). Arrowheads indicate the peak positions of the 20S and 26S proteasomes (open arrows, single-capped 26S; closed arrows, double-capped 26S). (*D*) Western blot analysis of fractionated total LCL extracts. Western blot analysis of proteasome subunits from fractions 1–32 fractionated in *C*. The sedimenting positions of the immature 20S, 20S, and 26S proteasomes are indicated by arrowheads. The mature and incompletely cleaved $β5i^{G201V}$ subunits are indicated by arrows. The mature β5i subunit is cleaved within a C-terminal polypeptide between Gly72 and Thr73. The insufficiently cleaved β5i subunit is probably cleaved at a site toward the N terminus site, yielding a fragment with a higher molecular weight. The same amount of protein was subjected to glycerol gradient ultracentrifugation. The level of proteasome is reduced in NNS patients. Control, LCL extract from healthy control; NNS, LCL extract from patient with NNS.

interface between β4 and β5i, which affected the surface contact of β5i with the adjacent β4 subunit (Fig. 2*B*). These results suggest that the G201V mutation affects both β5i catalytic activity and assembly of the 20S proteasome.

According to Sijts and Kloetzel (17), the β1 subunit has a caspase-like function, the β2 subunit has trypsin-like activity, and the β5 subunit has chymotrypsin-like activity. Although it has not been clearly confirmed which of the immunoproteasome subunits possess which peptidase activity, it is generally thought that β5i has chymotrypsin-like activity. We next examined the influence of the β5i mutation on proteasome peptidase activity. Extracts from immortalized lymphoblastoid cell lines (LCLs) that constitutively expressed the immunoproteasome, rather than the standard proteasome, were obtained from an NNS patient, his heterozygous parent, and a healthy control, and were separated by glycerol gradient centrifugation. The fractions were then assayed for chymotrypsin-like, trypsin-like, and caspase-like activity mediated by the 20S/26S proteasomes. The results showed that not only was chymotrypsin-like activity markedly decreased in NNS cells, but the other two enzyme-like activities were also decreased (Fig. 2*C*).

Reduced Proteasome Levels. To gain further insight into the molecular mechanisms affecting peptidase activity in the mutant cells, the glycerol density gradient fractions were subjected to Western blot analysis (Fig. 2*D*). Assembly of the mammalian 20S proteasome begins with the formation of the α-ring in conjunction with a dedicated assembly chaperone, PAC1-4. The β-ring is then formed on the α-ring with the aid of another chaperone, hUmp1, resulting in the formation of half-sized immature proteasomes. The immature proteasomes then dimerize to form the 20S proteasome accompanied by cleavage of β-subunit propeptides and the degradation of hUmp1 (9). Our most noteworthy finding was the accumulation of immature 20S proteasome precursors in NNS cells before incorporation of β5i and dimerization, as indicated by the presence of the proforms of β1i and β2i, α6 and hUmp1, and the absence of β5i (Fig. 2*D*, fractions 10–14) (18). Computer modeling suggests that this assembly defect could be due to the fact that β5i, β4, and β6 line up next to each other and that the interaction between mutant $β5i^{G201V}$ and β4 may be disturbed (Fig. 2*B*). The reduction in peptidase activity was unlikely due to differences in the ability of 20S to associate with 19S RP, because single-capped and double-capped 26S proteasomes were detected in the glycerol fractions from an NNS patient and control LCLs (Fig. 2*C*). The assembly defect caused a reduction in the number of 20S and 26S proteasomes in NNS cells (Fig. 2*D*), which accounts for the observed decrease in activity of all three peptidases. Another intriguing observation was that a portion of the $β5i^{G201V}$ subunit incorporated into the mature proteasome appeared as a slower migrating band, suggesting the presence of an insufficiently cleaved form of $β5i^{G201V}$ (Fig. 2*D*) (16). This may have contributed to the markedly reduced chymotrypsin-like activity seen in NNS cells compared with the other two peptidase activities.

Decreased Proteolytic Activity and Accumulation of Ubiquitinated and Oxidized Proteins. To examine proteolytic activity in vitro, the ornithine decarboxylase (ODC) degradation assay was performed (19). Proteolytic activity was significantly decreased in mutant proteasomes (Fig. 3*A*). As a consequence of the altered proteasome levels and incomplete cleavage of the subunits, proteolytic activity decreased and ubiquitinated proteins accumulated in LCLs (Fig. 3*B*) and fibroblasts from NNS patients (Fig. 3*C*). In particular, there was an obvious accumulation of K48 polyubiquitinated proteins in fibroblasts (Fig. 3*C*).

Because the immunoproteasome is important for degrading oxidized proteins and defective ribosomal products (20), we examined whether such proteins accumulated in NNS cells. We found that the level of oxidized proteins increased in cultured NNS fibroblasts and after stimulation with IFN-γ (Fig. 3*D*). Taken together, these results show that the G201V substitution within β5i severely impairs assembly of the immunoproteasome, leading to decreased proteasome levels and activity in β5i-expressing cells.

We then examined whether the defect in proteasome activity was apparent in situ in NNS patients. We stained skin biopsy sections obtained from an NNS patient and used sections from a monocytic fasciitis patient as a control. CD68 is a marker for monocyte/macrophages, a cell type known to predominantly express the immunoproteasome rather than the standard proteasome (21). Inflammatory responses characterized by the infiltration of numerous $CD68^+$ cells into the skin were observed in both NNS and fasciitis samples. However, the $CD68^+$ cells in the NNS sec-

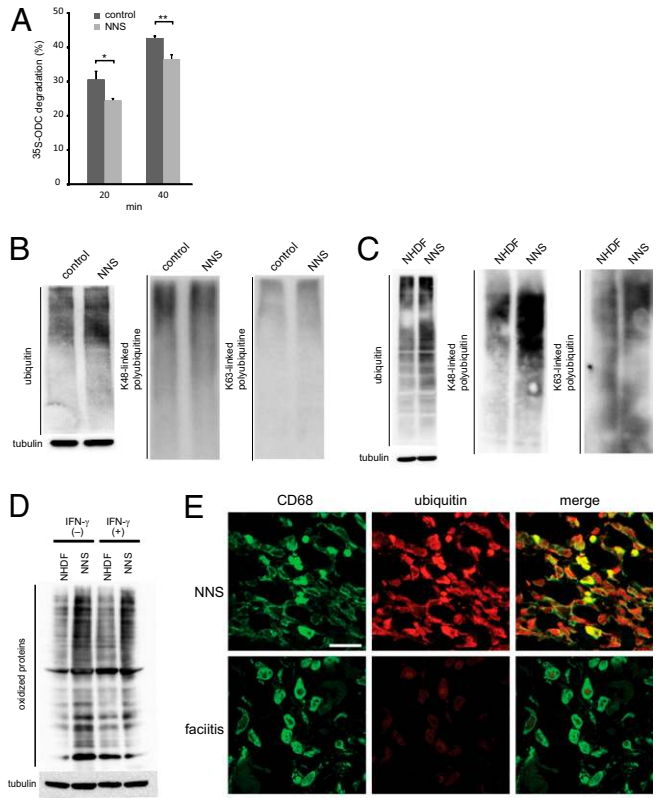

Fig. 3. Decrease of proteolytic activity and accumulation of polyubiquitinated and oxidized proteins in NNS cells. (*A*) In vitro proteolytic activity of the mutant proteasome. Degradation of recombinant ^{35}S-labeled ODC was expressed as % total ODC as described previously (11). Error bars indicated the SD of the mean ($n = 3$). *$P < 0.05$, **$P < 0.01$. (*B* and *C*) Accumulation of ubiquitinated proteins in LCLs (*B*) and fibroblasts (*C*). Western blot analysis of ubiquitinated proteins using an antiubiquitin antibody (*Left*), an anti-K48 polyubiquitinated protein antibody (*Middle*), and an anti-K63 polyubiquitinated protein antibody (*Right*). Tubulin was used as a loading control (*Lower*). NHDF, adult normal human dermal fibroblasts. (*D*) Levels of oxidized proteins determined by Oxyblot. NHDF and NNS fibroblasts were stimulated with or without 100 units of IFN-γ for 24 h. Tubulin was used as a loading control. (*E*) Immunofluorescence staining of CD68 and ubiquitinated proteins. Staining for CD68 (green) and ubiquitinated proteins (red) in skin sections from an NNS patient and a fasciitis patient. NNS ubiquitin signals showed a 4.7-fold increase with ImageJ (http://rsb.info.nih.gov/ij/) compared with fasciitis signals. (Scale bar, 10 μm.)

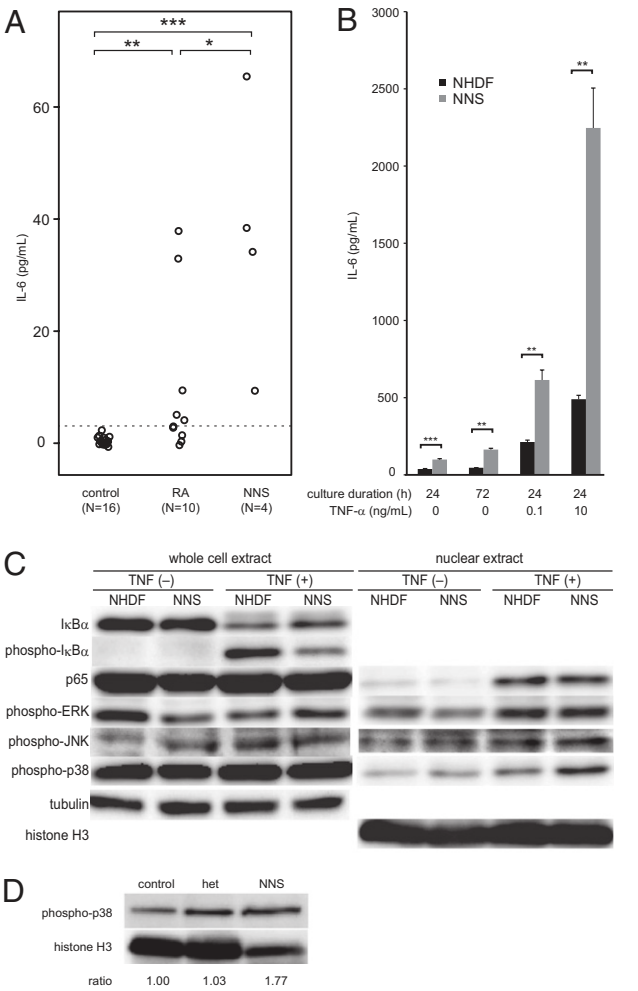

Fig. 4. Analyses of the level of IL-6 in NNS and the signal transduction system related to cytokine production. (*A*) IL-6 concentrations in sera from healthy controls, patients with NNS, and patients with rheumatoid arthritis. IL-6 levels in sera were determined by ELISA. (*B*) IL-6 production by cultured fibroblasts. The concentrations of IL-6 in conditioned media were determined by ELISA (in triplicate). (*C*) Western blot analysis for NF-κB and MAPK. Whole cell extracts and nuclear extracts were immunoblotted using antibodies against IκBα, p-IκBα, p65, p-ERK, p-JNK, and p-p38. (*D*) Western blot analysis of p-p38 in peripheral blood lymphocytes. Nuclear extracts from the peripheral blood lymphocytes of a healthy control, a heterozygous family member, and a NNS patient were blotted and visualized with anti–p-p38. Error bars indicate SD of the mean. *$P < 0.05$, **$P < 0.01$, ***$P < 0.001$ [Mann-Whitney *u* test (*A*) and two-tailed Welch's *t* test (*B*)]. Signal intensities were quantified using ImageJ and expressed as fold changes relative to a healthy control normalized to histone H3 (*D*).

tions were strongly positive for ubiquitin, whereas ubiquitin was only faintly detectable in the fasciitis sections (Fig. 3*E*).

Increased IL-6 and IP-10 Levels in NNS Patient Sera and Signal Transduction in NNS Fibroblasts. We next screened NNS patient sera for inflammatory cytokines using a multiplex bead-based ELISA on a suspension array. The results showed a significant increase in the levels of interleukin (IL)-6, IFN-γ–inducible protein (IP)-10, granulocyte colony stimulating factor, and monocyte chemoattractant protein-1 (Fig. S3*A*). IL-6 was of particular interest because it is a pleiotropic cytokine with a wide range of biological activities, and it plays a key role of immune regulation, hematopoiesis, oncogenesis, and inflammation (22–24). Increased IL-6 levels in NNS sera were confirmed using a standard ELISA (Fig. 4*A*). IL-6 production was significantly higher in NNS patient fibroblasts than in healthy control fibroblasts both in the presence and absence of TNF-α (Fig. 4*B*). The serum concentration of IP-10 was also higher than that in healthy controls (Fig. S3 *A* and *B*). We measured the level of IP-10 in conditional media from cultured fibroblasts using an ELISA, but found no significant difference under the conventional culture condition, although NNS cells tended to overproduce IP-10 after stimulation with 10 ng/mL TNF-α (Fig. S3*C*).

We next investigated the various signal transduction pathways that could be responsible for IL-6 overproduction by NNS fibroblasts. Nuclear factor (NF)-κB and AP-1 are the two major transcription factors that induce proinflammatory cytokines, including IL-6 (25, 26). We used an EMSA to detect activated NF-κB in cells treated with TNF-α; however, no differences in the amount of the p65/p50 heterodimer were observed in nuclear extracts from NNS fibroblasts and healthy control fibroblasts (Fig. S4 *A* and *B*). Consistent with this result, IκBα degradation and nuclear translocation of NF-κB were not enhanced in NNS fibroblasts (Fig. 4*C*). Although activation of NF-κB is largely dependent on the ubiquitin–proteasome system, these results

suggest that decreased proteasome activity does not have much influence on the regulation of NF-κB signaling in NNS cells.

We next measured the molecules that activate AP-1, including JNK1/2/3, ERK1/2, and p38, by Western blot analysis (27, 28). The amount of phosphorylated p38 (p-p38) in the nuclear extracts from NNS fibroblasts was increased (Fig. 4*C*), irrespective of TNF-α stimulation; however, there was no obvious difference in the levels of JNK1/2/3 and ERK1/2 (Fig. 4*C*). We also observed increased levels of p-p38 in the nuclear extracts from NNS peripheral blood lymphocytes (Fig. 4*D*). The build-up of oxidized proteins and/or reactive oxygen species (ROS) within NNS fibroblasts may be one of the mechanisms responsible for the accumulation of p-p38 (29, 30).

Discussion

We have identified a point mutation in the gene encoding the immunoproteasome subunit β5i as the cause of NNS. This mutation interferes with the assembly of the 20S proteasome in cells expressing immunoproteasomes. The mutation is described as c.602G > T, and results in a Gly201 to Val (G201V) (NM_148919) substitution in the immunoproteasome β5i subunit. Although a heterozygous carrier showed reduced proteasome peptidase activity, carriers had no clinical symptoms. Thus, the NNS phenotype may be due to a reduction in total proteasome enzymatic activity below the threshold necessary for maintaining cellular homeostasis in homozygous individuals.

The *PSMB8* mutation, c.224C > T (Thr75Met), occurs in patients with JMP syndrome (13). Mutant β5i in JMP patients results in a clear reduction in chymotrypsin-like activity only, with no disruption of other peptidase activities. However, the G201V mutation we identified in NNS patients causes losses of all peptidase activity owing to assembly defects and reduced proteasome levels. The T75M mutation is probably rapidly incorporated to the proteasome complex during biogenesis and is specific for chymotrypsin-like activity. The differences between the JMP syndrome and NNS phenotypes, including cytokine production by various cells during inflammatory or noninflammatory states, need to be clarified because these differences could result from a reduction in chymotrypsin-like activity in JMP syndrome or from reductions in chymotrypsin-, trypsin-, and caspase-like activity in NNS. One of the main differences between NNS and JMP syndrome is the level of IFN-γ. IFN-γ levels are increased in JMP patients, but are within the normal range in NNS patients (Fig. S3*A*). The basis for this difference is unclear. It is possible that IFN-γ levels may not increase when all three peptidase activities are inhibited.

We also found increased IP-10 levels in patient sera using ELISA on suspension arrays. There were no significant differences in IP-10 levels between nonstimulated NNS fibroblasts and control cells, although NNS fibroblasts tended to overproduce IP-10 after stimulation with TNF-α (Fig. S3 *B* and *C*). This may reflect the proinflammatory state in NNS cells, or an increased sensitivity to cytokines (31). Because IP-10 is categorized as an inflammatory chemokine produced by various types of cells, it may play an important role in leukocyte homing to inflamed tissues and in perpetuating inflammation in various autoimmune diseases such as rheumatoid arthritis, systemic lupus erythematosus, systemic sclerosis, and multiple sclerosis (32). Thus, IP-10 may enhance inflammation in NNS patients and be associated with the autoantibody production that is occasionally observed.

A single base deletion in the 5′-UTR of hUmp1 causes keratosis linearis with ichthyosis congenita and sclerosing keratoderma (KLICK) syndrome, which is characterized by palmoplantar keratoderma (33) related to proteasome activity. This mutation results in changes in hUmp1 levels and alterations in the epidermal distribution of hUmp1 and proteasomal subunits. It is unclear how the proteasome functions in KLICK syndrome, although it is clear that disturbances in proteasome function cause clinical phenotypes in humans.

Studies in animal models indicate that cells deficient in various immunoproteasome subunits show poor CD8 responses when challenged with epitopes (34, 35) and may display alterations in the T-cell receptor (TCR) repertoire (36). In particular, β5i-deficient mice show increased susceptibility to pathogens, most likely due to the reduced efficiency of antigen presentation by β5i-deficient cells (12). Actually, in NNS patients, unresponsiveness to an intradermally applied purified protein derivative of *Mycobacterium tuberculosis* has been reported; however, there are no documented changes in susceptibility to pathogens, and no abnormalities in the number of any particular T-cell subset have been observed, apart from reduced NK activity (4). Conversely, there are no reports that β5i-deficient mice show the type of systemic inflammation observed in NNS patients.

In general, gene-deficient mice are very useful tools for analyzing the functions of target genes; however, the $\beta5i^{G201V}$ mutation shows a type of "enzymatic dominant-negative interference," which abrogates not only chymotrypsin-like activity (due to the mutation) but also the activity of the entire proteasome (due to defective assembly). Thus, it is not surprising that the phenotype seen in NNS is different from that seen in *Psmb8* knockout mice (12, 20) or after treatment with PR-957 inhibitors (37). Thus, analysis of patients with NNS and JMP syndrome and mice knocked in with these mutations would provide new insights into the function of the immunoproteasome in vivo.

Finally, we observed increased levels of p-p38 in nuclear extracts from NNS peripheral blood lymphocytes (Fig. 4*D*), although it remains unknown precisely how attenuation of proteasome activity causes accumulation of p-p38 in the nucleus. The

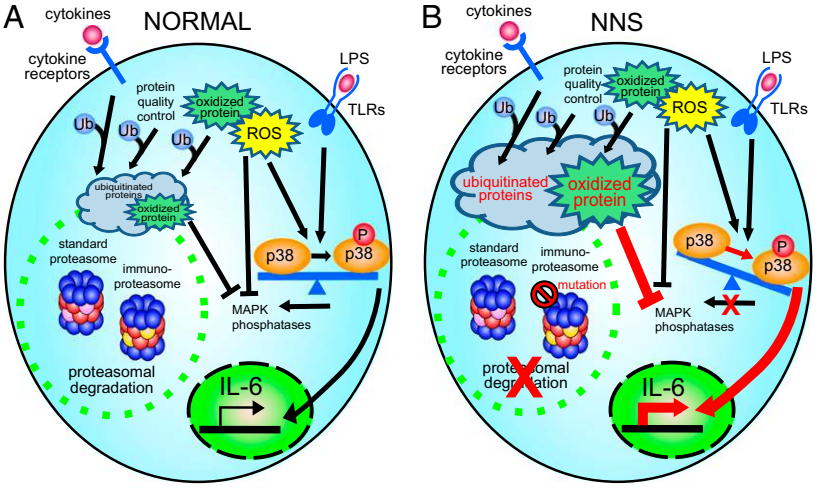

Fig. 5. Schematic model showing induction of inflammation in NNS patients with the *PSMB8* mutation. Our data are based on the scheme proposed by Bulua et al. (40). (*A*) In a normal cell, ubiquitinated or oxidized proteins generated by various stressors, including cytokines, are cleared by proteasomes. (*B*) The ubiquitinated and oxidized proteins accumulate in a cell with the *PSMB8* mutation (NNS cell). ROS and/or oxidized proteins may cause phosphorylation of p-38 to predominate over the nonphosphorylated form by inhibiting MAPK phosphatase or by activating MAPK.

accumulation of oxidized proteins and/or ROS in NNS fibroblasts may be one of the mechanisms responsible for the accumulation of p-p38 (29, 30, 38, 39). Increased p-p38 levels are in agreement with the proposed mechanism for TNFR1-associated periodic syndrome (TRAPS), which is another autoinflammatory syndrome (40).

To date, proteasome inhibitors have been used clinically to treat multiple myeloma and mantle cell lymphoma and are also effective for experimental autoimmune and inflammatory phenotypes, such as arthritis (37) and systemic lupus erythematosus (41). Generally, it is said that proteasome inhibitors induce apoptosis and inhibit immune responses. However, our results indicate that inhibiting the immunoproteasome can induce inflammatory reactions under some circumstances. In this context, the *PSMB8* mutation in NNS can be mimicked by histiocytoid Sweet syndrome (42) and cutaneous vasculitis (43) induced by bortezomib, a nonspecific proteasome inhibitor.

Taken together, the data in the present study suggest that reduction in proteasome activity affects signal transduction and promotes inflammation (Fig. 5). In NNS patients with the *PSMB8* mutation, inflammation causes ubiquitinated proteins to accumulate (compounding the effects on joints, skin, and muscle). These intracellular aggregates may then trigger innate immune responses and increased ROS production (increasing the levels of oxidized proteins), which then, through the activity of p-p38, activate the AP1 transcription factor causing an increase in the secretion of various cytokines such as IL-6.

Materials and Methods

Homozygosity Mapping. The genome-wide ROH overlap pattern was detected using in-house Ruby script (available on request) (44).

Glycerol Density Gradient Separation. Proteins from cell extracts (600 ìg) were separated into 32 fractions by centrifugation (22 h at 100,000 × *g*) in 8 -32 % (vol/vol) linear glycerol gradients.

Additional materials and methods are available in *SI Materials and Methods*.

ACKNOWLEDGMENTS. We thank the families for their participation. We also thank Prof. M. Nakashima for valuable discussion and Ms. C. Hayashida and M. Ohga for technical assistance. This work was supported, in part, by grants from the Ministry of Health, Labour, and Welfare (to F.F., N.K, and K.-i.Y.), the Japan Society for the Promotion of Science (22591094 to H.I., 21390100 to K.-i.Y., 20590331 to A. Kinoshita, 21791566 to H.M., 23791115 to K.A., and 23591651 to N.K.), the Takeda Scientific Foundation and the Naito Foundation (K.i.-Y.), and the Lydia O'Leary Memorial Foundation (N.K.).

1. Nakajo A (1939) Secondary hypertrophic osteoperiostosis with pernio. *J Dermatol Urol* 45:77–86.
2. Nishimura N, Deki T, Kato S (1950) Secondary hypertrophic osteoperiostosis with pernio-like skin lesions observed in two families. *J Dermatol Venereol* 60:136–141.
3. Kitano Y, Matsunaga E, Morimoto T, Okada N, Sano S (1985) A syndrome with nodular erythema, elongated and thickened fingers, and emaciation. *Arch Dermatol* 121: 1053–1056.
4. Tanaka M, et al. (1993) Hereditary lipo-muscular atrophy with joint contracture, skin eruptions and hyper-gamma-globulinemia: A new syndrome. *Intern Med* 32:42–45.
5. Horikoshi A, Iwabuchi S, Iizuka Y, Hagiwara T, Amaki I (1980) A case of partial lipodystrophy with erythema, dactylic deformities, calcification of the basal ganglia, immunological disorders, and low IQ level (Translated from Japanese). *Rinsho Shinkeigaku* 20:173–180.
6. Kasagi S, et al. (2008) A case of periodic-fever-syndrome-like disorder with lipodystrophy, myositis, and autoimmune abnormalities. *Mod Rheumatol* 18:203–207.
7. Oyanagi K, et al. (1987) An autopsy case of a syndrome with muscular atrophy, decreased subcutaneous fat, skin eruption and hyper gamma-globulinemia: Peculiar vascular changes and muscle fiber degeneration. *Acta Neuropathol* 73:313–319.
8. Muramatsu T, Sakamoto K (1987) Secondary hypertrophic osteoperiostosis with pernio (Nakajo). *Skin Res* 29:727–731.
9. Murata S, Yashiroda H, Tanaka K (2009) Molecular mechanisms of proteasome assembly. *Nat Rev Mol Cell Biol* 10:104–115.
10. Jung T, Catalgol B, Grune T (2009) The proteasomal system. *Mol Aspects Med* 30: 191–296.
11. Tanaka K (2009) The proteasome: Overview of structure and functions. *Proc Jpn Acad Ser B Phys Biol Sci* 85:12–36.
12. Fehling HJ, et al. (1994) MHC class I expression in mice lacking the proteasome subunit LMP-7. *Science* 265:1234–1237.
13. Agarwal AK, et al. (2010) PSMB8 encoding the β5i proteasome subunit is mutated in joint contractures, muscle atrophy, microcytic anemia, and panniculitis-induced lipodystrophy syndrome. *Am J Hum Genet* 87:866–872.
14. Garg A, et al. (2010) An autosomal recessive syndrome of joint contracture, muscular atrophy, microcytic anemia, and panniculitis-associated lipodystrophy. *J Clin Endocrinol Metab* 95:E48–E63.
15. Unno M, et al. (2002) The structure of the mammalian 20S proteasome at 2.75 A resolution. *Structure* 10:609–618.
16. Seemuller E, Lupas A, Baumeister W (1996) Autocatalytic processing of the 20S proteasome. *Nature* 382:468–471.
17. Sijts EJAM, Kloetzel P-M (2011) The role of the proteasome in the generation of MHC class I ligands and immune responses. *Cell Mol Life Sci* 68:1491–1502.
18. Hirano Y, et al. (2008) Dissecting beta-ring assembly pathway of the mammalian 20S proteasome. *EMBO J* 27:2204–2213.
19. Hirano Y, et al. (2005) A heterodimeric complex that promotes the assembly of mammalian 20S proteasomes. *Nature* 437:1381–1385.
20. Seifert U, et al. (2010) Immunoproteasomes preserve protein homeostasis upon interferon-induced oxidative stress. *Cell* 142:613–624.
21. Froment C, et al. (2005) A quantitative proteomic approach using two-dimensional gel electrophoresis and isotope-coded affinity tag labeling for studying human 20S proteasome heterogeneity. *Proteomics* 5:2351–2363.
22. Akira S, Taga T, Kishimoto T (1993) Interleukin-6 in biology and medicine. *Adv Immunol* 54:1–78.
23. Kishimoto T (2005) Interleukin-6: From basic science to medicine—40 years in immunology. *Annu Rev Immunol* 23:1–21.
24. Nishimoto N, Kishimoto T (2006) Interleukin 6: From bench to bedside. *Nat Clin Pract Rheumatol* 2:619–626.
25. Gyrd-Hansen M, Meier P (2010) IAPs: From caspase inhibitors to modulators of NF-kappaB, inflammation and cancer. *Nat Rev Cancer* 10:561–574.
26. Pasparakis M (2009) Regulation of tissue homeostasis by NF-kappaB signalling: Implications for inflammatory diseases. *Nat Rev Immunol* 9:778–788.
27. Thalhamer T, McGrath MA, Harnett MM (2008) MAPKs and their relevance to arthritis and inflammation. *Rheumatology (Oxford)* 47:409–414.
28. Kumar S, Boehm J, Lee JC (2003) p38 MAP kinases: Key signalling molecules as therapeutic targets for inflammatory diseases. *Nat Rev Drug Discov* 2:717–726.
29. Kamata H, et al. (2005) Reactive oxygen species promote TNFalpha-induced death and sustained JNK activation by inhibiting MAP kinase phosphatases. *Cell* 120: 649–661.
30. Park GB, et al. (2010) Endoplasmic reticulum stress-mediated apoptosis of EBV-transformed B cells by cross-linking of CD70 is dependent upon generation of reactive oxygen species and activation of p38 MAPK and JNK pathway. *J Immunol* 185: 7274–7284.
31. Villagomez MT, Bae SJ, Ogawa I, Takenaka M, Katayama I (2004) Tumour necrosis factor-α but not interferon-γ is the main inducer of inducible protein-10 in skin fibroblasts from patients with atopic dermatitis. *Br J Dermatol* 150:910–916.
32. Lee EY, Lee Z-H, Song YW (2009) CXCL10 and autoimmune diseases. *Autoimmun Rev* 8:379–383.
33. Dahlqvist J, et al. (2010) A single-nucleotide deletion in the POMP 5′ UTR causes a transcriptional switch and altered epidermal proteasome distribution in KLICK genodermatosis. *Am J Hum Genet* 86:596–603.
34. Caudill CM, et al. (2006) T cells lacking immunoproteasome subunits MECL-1 and LMP7 hyperproliferate in response to polyclonal mitogens. *J Immunol* 176:4075–4082.
35. Hutchinson S, et al. (2011) A dominant role for the immunoproteasome in CD8+ T cell responses to murine cytomegalovirus. *PLoS ONE* 6:e14646.
36. Basler M, Moebius J, Elenich L, Groettrup M, Monaco JJ (2006) An altered T cell repertoire in MECL-1-deficient mice. *J Immunol* 176:6665–6672.
37. Muchamuel T, et al. (2009) A selective inhibitor of the immunoproteasome subunit LMP7 blocks cytokine production and attenuates progression of experimental arthritis. *Nat Med* 15:781–787.
38. Hou N, Torii S, Saito N, Hosaka M, Takeuchi T (2008) Reactive oxygen species-mediated pancreatic beta-cell death is regulated by interactions between stress-activated protein kinases, p38 and c-Jun N-terminal kinase, and mitogen-activated protein kinase phosphatases. *Endocrinology* 149:1654–1665.
39. McCubrey JA, Lahair MM, Franklin RA (2006) Reactive oxygen species-induced activation of the MAP kinase signaling pathways. *Antioxid Redox Signal* 8:1775–1789.
40. Bulua AC, et al. (2011) Mitochondrial reactive oxygen species promote production of proinflammatory cytokines and are elevated in TNFR1-associated periodic syndrome (TRAPS). *J Exp Med* 208:519–533.
41. Neubert K, et al. (2008) The proteasome inhibitor bortezomib depletes plasma cells and protects mice with lupus-like disease from nephritis. *Nat Med* 14:748–755.
42. Murase JE, et al. (2009) Bortezomib-induced histiocytoid Sweet syndrome. *J Am Acad Dermatol* 60:496–497.
43. Gerecitano J, et al. (2006) Drug-induced cutaneous vasculitis in patients with non-Hodgkin lymphoma treated with the novel proteasome inhibitor bortezomib: A possible surrogate marker of response? *Br J Haematol* 134:391–398.
44. Kurotaki N, et al. (2011) Identification of novel schizophrenia Loci by homozygosity mapping using DNA microarray analysis. *PLoS ONE* 6:e20589.

Supporting Information

Arima et al. 10.1073/pnas.1106015108

SI Materials and Methods

DNA and Cell Samples. Genomic DNA was isolated from peripheral blood white cells using a conventional phenol-chloroform method combined with dialysis purification. B cells obtained from peripheral blood were transformed using Epstein-Barr virus.

SNP Genotyping. DNA samples were analyzed using the GeneChip Human Mapping 500K array set (Nsp and Sty arrays) according to the manufacturer's protocol (Affymetrix). Raw array intensity data (CEL files) of 8 of our samples and International HapMap Project phase II Japanese (JPT) samples ($n = 45$) were genotyped simultaneously using BRLMM genotyping software.

SNP Microarray-Based Homozygosity Mapping. To detect the genome-wide structure of ROHs, SNP genotype files (CHP files) were analyzed using the "unpaired LOH detection" function in the Partek Genomics Suite (GS). To obtain maximum resolution for ROH detection, no SNP heterozygosity baseline files were used. We adopted the following thresholds for ROH: 1.0 Mb for first-cousin marriage offspring (patients 2 and 4), 750 kb for other consanguineous marriage offspring (patients 1 and 3), and 500 kb for nonconsanguineous marriage offspring (patient 5). No filtration was used for the unaffected siblings of patient 4. The genome-wide ROH overlap pattern was detected using in-house Ruby script (1) (available on request) and visualized using Partek GS. A region showing ROHs for all of the patients, but not the unaffected siblings, was considered to be a candidate region.

Mutation Search and Sequencing. All PCR reactions used genomic DNA with KOD FX (Toyobo) or ExTaq DNA polymerase HS (Takara) at the appropriate annealing temperature. PCR products were purified for direct sequencing using Exonuclease I (Epicentre) and shrimp alkaline phosphatase (GE Healthcare). Sequencing reactions used a BigDye Terminator v3.1 Cycle Sequencing kit (Applied Biosystems) and electrophoresed using Autosequencer Model 3130xl.

Structural Modeling. Structural models of mutated and nonmutated immunoproteasomes were constructed by exchanging the residues from the constitutive subunits (2) with those from the inducible subunits. Several of the generated models that had minimum energies were further subjected to an experimental data-free energy minimization process using a Crystallography and NMR system (3).

Cell Culture. LCLs and skin fibroblasts were cultured in RPMI 1640 and DMEM, respectively, supplemented with 10% FBS, 100 IU/mL penicillin G, and 100 mg/mL streptomycin.

Protein Extracts, Immunological Analysis, and Antibodies. Cells were lysed in ice-cold lysis buffer [50 mM Tris-HCl (pH 7.5), 0.5% (vol/vol) Nonidet P-40, and 1 mM DTT with 2 mM ATP and 5 mM $MgCl_2$]. The extracts were clarified by centrifugation at 20,000 × *g* for 10 min at 4 °C. The supernatants were subjected to SDS/PAGE (12.5% for proteasome subunits or 7.5% for polyubiquitinated proteins) or analyzed by glycerol gradient centrifugation. The separated proteins were transferred onto a polyvinylidene difluoride membrane and incubated with the indicated antibodies. Membranes were developed using the ECL Plus Western Blotting Detection system (GE Healthcare).

Antibodies against proteasome β1, β2, β5, β7, β1i, β2i, and β5i subunits and hUmp-1 were raised in rabbits using recombinant proteins (4). An anti-β4 subunit monoclonal antibody (mAb), anti-Rpt6 mAb, and anti-α6 subunit mAb (MCP20) were purchased from ENZO. An antiubiquitin antibody (Dako), anti–K48- and anti–K63-linked ubiquitin antibodies (Millipore) (4), horseradish peroxidase (HRP)-conjugated antimouse, and antirabbit IgG antibodies (Jackson ImmunoResearch Laboratories) were used for Western blot analysis.

Glycerol Density Gradient Separation. Proteins from cell extracts (600 μg) were separated into 32 fractions by centrifugation (22 h at 100,000 × *g*) in 8–32% (vol/vol) linear gradients as described previously (6).

Assays for Proteasome Peptidase Activities. Chymotrypsin-like, trypsin-like, and caspase-like activities were determined using the fluorescent peptide substrates succinyl-Leu-Leu-Val-Tyr-7-amido-4-methylcoumarin (Suc-LLVY-MCA), butyloxycarbonyl-Leu-Arg-Arg-4-metylcoumarin (Boc-LRR-MCA), and benzyloxycarbonyl-Leu-Leu-Glu-methylcoumarylamine (Z-LLE-MCA), as described previously (7). The assays for chymotrypsin-like and caspase-like activities were carried out in the presence of 0.03% SDS, which is a potent artificial activator of the latent 20S proteasome.

Assays for Proteolytic Degradation in Vitro. Degradation of the recombinant 35S-labeled ornithine decarboxylase (ODC) was assayed in the presence of ATP, at 20 min and 40 min, as described previously (8). Data were shown in ^{35}S-ODC degradation (%).

Oxidized Protein Detection. Oxidized proteins were visualized using an OxyBlot protein oxidization detection kit (Millipore) following the supplier's protocol.

Immunohistochemistry. Immunohistochemistry used a standard indirect immunofluorescence method. Sections of formalin-fixed, paraffin-embedded tissues were deparaffinized and microwave epitope retrieval was performed after pretreatment at 80 °C for 30 min in 10 mM citrate buffer (pH 6.0). Endogenous peroxidase was inactivated with a 3% H_2O_2 solution following epitope retrieval. After blocking in 5% normal horse serum in PBS, the slides were incubated for 60 min at room temperature with rabbit polyclonal antiubiquitin antibodies (Dako) or a mouse monoclonal antihuman CD68 antibody (ProSci).

Sections were then incubated with FITC-conjugated donkey antimouse IgG or tetramethylrhodamine isothiocyanate-conjugated donkey antirabbit IgG (Jackson ImmunoResearch) in 5% normal horse serum in PBS for 30–45 min at room temperature. After washing in PBS, the slides were mounted in Vectashield mounting medium (Vector Laboratories) and scanned by confocal microscopy (LSM5, PASCAL; Carl Zeiss). Control experiments were performed to ensure the isotype specificity for each of the secondary antibodies. Negative control studies used species-specific IgG as primary antibodies.

Electrophoretic Mobility Shift Assay (EMSA) Using NF-κB Consensus Oligonucleotides. Nuclear proteins were extracted using a Nuclear Extract kit (Active Motif). Nuclear extracts (4 μg) were used for the EMSA assay using an EMSA kit (Pierce). The consensus oligonucleotide sequences for the NF-κB binding motif were: 5′-AGT TGA GGG GAC TTT CCC AGG C-3′ (sense) and 5′-GCCTGGGAAAGTCCCCTCAACT-3′ (antisense). For the competition assay, a nuclear extract was preincubated with an unlabeled oligonucleotide followed by addition of a [γ-^{32}P]-ATP labeled NF-κB probe. Samples were loaded onto 4% polyacrylamide gels (38:1) in 0.5 × TBE and run at 1 W at room

temperature. Gels were dried and exposed to a Storage Phosphor Screen BAS-IP (GE Healthcare). To confirm the integrity of NF-κB binding, anti-p65 and anti-p50 (Santa Cruz Biotechnology) antibodies were used for the supershift assay.

1. Kurotaki N, et al. (2011) Identification of novel schizophrenia Loci by homozygosity mapping using microarray analysis. *PLoS ONE* 6:e20589.
2. Unno M, et al. (2002) The structure of the mammalian 20S proteasome at 2.75 A resolution. *Structure* 10:609–618.
3. Brünger AT, et al. (1998) Crystallography & NMR system: A new software suite for macromolecular structure determination. *Acta Crystallogr D Biol Crystallogr* 54: 905–921.
4. Hirano Y, et al. (2008) Dissecting beta-ring assembly pathway of the mammalian 20S proteasome. *EMBO J* 27:2204–2213.
5. Newton K, et al. (2008) Ubiquitin chain editing revealed by polyubiquitin linkage-specific antibodies. *Cell* 134:668–678.
6. Hirano Y, Murata S, Tanaka K (2005) Large- and small-scale purification of mammalian 26S proteasomes. *Methods Enzymol* 399:227–240.
7. Murata S, et al. (2007) Regulation of CD8+ T cell development by thymus-specific proteasomes. *Science* 316:1349–1353.
8. Hirano Y, et al. (2005) A heterodimeric complex that promotes the assembly of mammalian 20S proteasomes. *Nature* 437:1381–1385.
9. Feng DF, Doolittle RF (1987) Progressive sequence alignment as a prerequisite to correct phylogenetic trees. *J Mol Evol* 25:351–360.

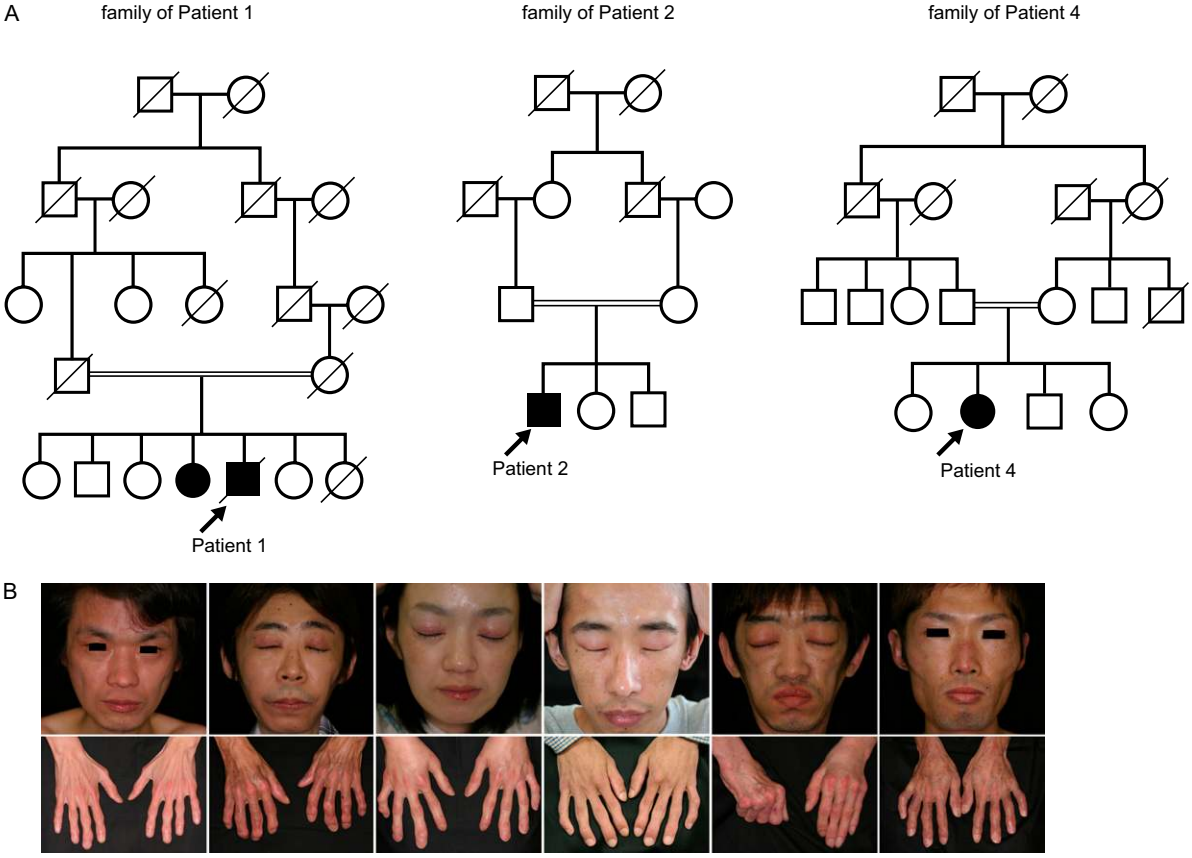

Fig. S1. (Continued)

C

	Patient 1	Patient 2	Patient 3	Patient 4	Patient 5	Patient 6	Patient 7	patient's father	Control 1	Control 2	Control 3	Control 4	Control 5	Control 6	Control 7
rs2857103	TT	TT	TT	TT	TT	TT	TT	TT	TT	GG	GT	GG	GG	GT	TT
rs10484565	GG	GG	GG	GG	GG	GG	GG	GG	AG	AG	GG	GG	GG	GG	GG
rs4148876	GG	GG	GG	GG	GG	GG	GG	GG	GA	AA	GA	AA	AA	GG	GG
rs241439	AA	AA	AA	AA	AA	AA	AA	AA	AA	AA	AA	AC	AC	AC	AA
rs241439	CC	CC	CC	CC	CC	CC	CC	CC	AC	AC	AC	AC	AA	AC	CC
rs241433	GG	GG	GG	GG	GG	GG	GG	GA	GA	GG	AA	GG	GA	GG	GA
rs241433	TT	TT	TT	TT	TT	TT	TT	TT	TT	GT	TT	GG	GT	GT	TT
rs4148872	GG	GG	GG	GG	GG	GG	GG	GG	GG	GG	GG	GG	GG	GA	GG
rs241429	CC	CC	CC	CC	CC	CC	CC	CC	CC	TC	CC	TT	TC	TC	CC
rs3819717	TT	TT	TT	TT	TT	TT	TT	TC	TC	TC	CC	TT	TC	TT	TC
rs241425	TT	TT	TT	TT	TT	TT	TT	TC	TC	CC	TT	CC	TC	TC	TT
rs4148870	AA	AA	AA	AA	AA	AA	AA	AA	GA	GA	GA	AA	GA	GA	GG
rs4713598	TT	TT	TT	TT	TT	TT	TT	TG	TG	TG	TT	GG	TG	TG	TT
rs3763366	CC	CC	CC	CC	CC	CC	CC	CC	CG	CG	GG	CC	CG	CG	GG
rs3763364	TT	TT	TT	TT	TT	TT	TT	TA	TT	TT	TT	AA	TT	TT	TT
rs3763349	CC	CC	CC	CC	CC	CC	CC	CC	TC	TC	TT	CC	TC	TC	TT
PSMB8 exon 5	TT	TT	TT	TT	TT	TT	TT	TG	GG	GG	GG	GG	GG	GG	GG
rs9357155	GG	GG	GG	GG	GG	GG	GG	GA	GA	GG	GG	GG	GG	GG	GG
rs9276810	GG	GG	GG	GG	GG	GG	GG	GA	GA	GG	GG	AA	GA	GA	GG
rs6924102	AA	AA	AA	AA	AA	AA	AA	AG	AG	AG	AA	GG	AG	AG	AA
rs4713599	CC	CC	CC	CC	CC	CC	CC	CA	AA	AA	AA	AA	AA	AA	AA
rs2071543	CC	CC	CC	CC	CC	CC	CC	CA	CA	CC	CC	CC	CC	CC	CC
rs2071463	GG	GG	GG	GG	GG	GG	GG	GG	AG	GG	AA	GG	AG	GG	AG
rs2071541	CC	CC	CC	CC	CC	CC	CC	CT	TT	CT	TT	TT	TT	TT	TT
rs2071540	GG	GG	GG	GG	GG	GG	GG	GG	AG	GG	AA	GG	AG	AG	AA
rs1057373	TT	TT	TT	TT	TT	TT	TT	TG	GG	TG	GG	GG	GG	GG	GG
rs4711312	GG	GG	GG	GG	GG	GG	GG	GA	AA	GA	AA	AA	AA	AA	AA
rs735883	CC	CC	CC	CC	CC	CC	CC	CT	CT	CT	CC	TT	CT	CT	CC
rs2071482	TT	TT	TT	TT	TT	TT	TT	TG	GG	TG	GG	GG	GG	GG	GG
rs4148882	TT	TT	TT	TT	TT	TT	TT	TT	TC	TT	CC	TT	TC	TC	CC
rs12527715	CC	CC	CC	CC	CC	CC	CC	CT	TT	CT	TT	TT	TT	TT	TT
rs12529313	GG	GG	GG	GG	GG	GG	GG	GA	AA	GA	AA	AA	AA	AA	AA
rs2395269	GG	GG	GG	GG	GG	GG	GG	GT	TT	GT	TT	TT	TT		
rs2071538	CC	CC	CC	CC	CC	CC	CC	CC	CC	CC	TC	CC	TC	TC	TC
rs4148880	GG	GG	GG	GG	GG	GG	GG	GA	AA	GA	AA	AA	AA	AA	AA
rs1351383	GG	GG	GG	GG	GG	GG	GG	GT	TT	GG	TT	GG	GT	GT	TT

Fig. S1. (Continued)

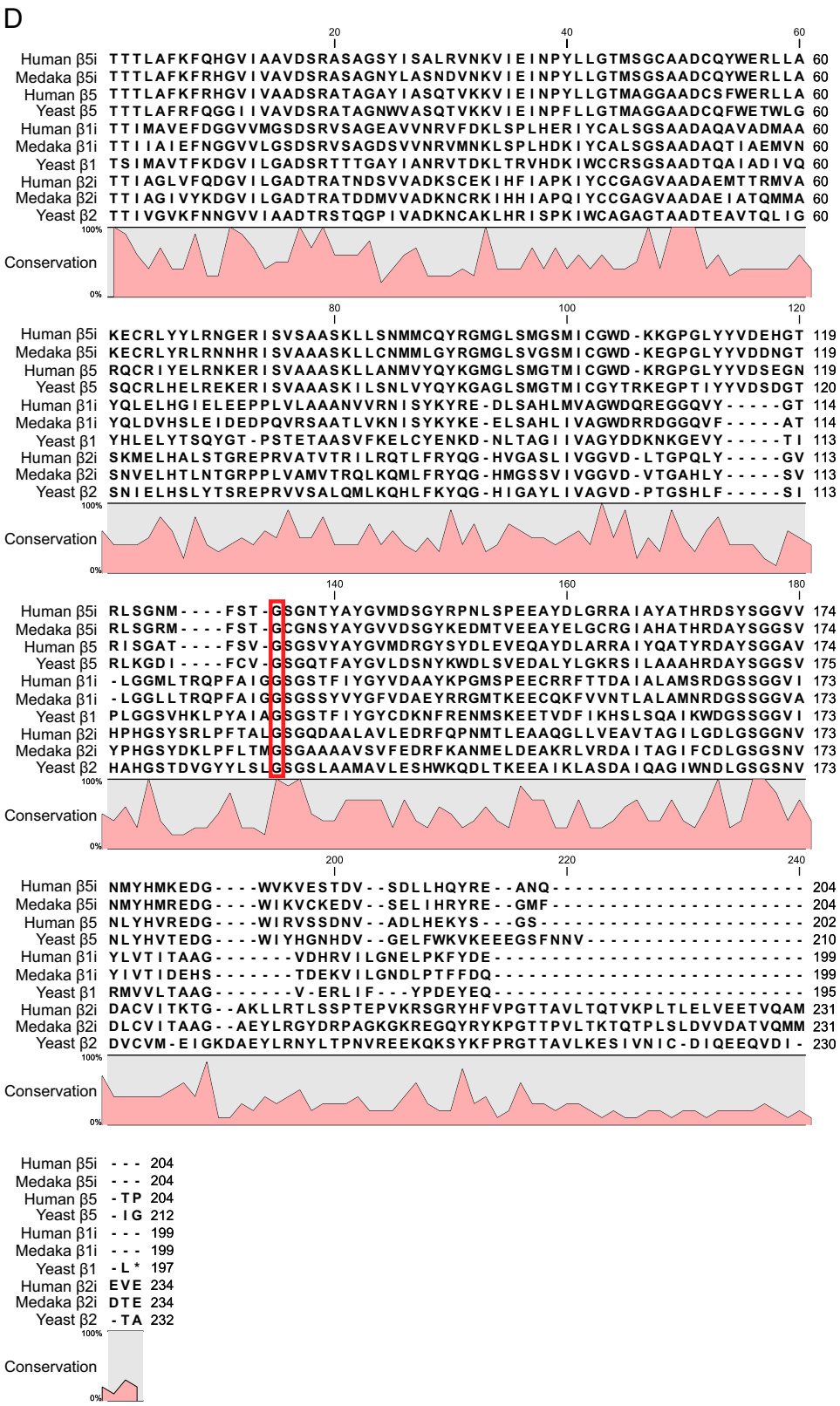

Fig. S1. NNS patients and their consanguineous family histories. (*A*) The families of patients 1, 2, and 4 contain offspring from consanguineous marriages. Solid circles and squares indicate patients with NNS. Arrows, double lines, and diagonal lines indicate probands, consanguineous marriages, and deceased individuals, respectively. (*B*) Photograph of the characteristic thin facial appearance and elongated clubbed fingers in patients 2–7. (*C*) Haplotypes around the *PSMB8* gene mutation. SNPs around *PSMB8* exon 5 were genotyped for seven NNS patients, the father of one patient, and nine controls. All patients shared the same haplotype within this region, which suggests that this mutation was transmitted from a single founder. Control: healthy control in general population. (*D*) Evolutionary conservation of proteasome subunits β5i, β5, β1i, β1, β2i, and β2. Each amino acid sequence is shown in its mature form. The red box indicates the position of the NNS mutation. Multiple amino acid sequence alignment using CLC Sequence Viewer version 6.4, implementing the progressive alignment algorithm (9).

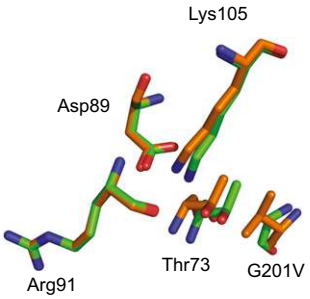

Fig. S2. Computer modeling of mutant β5i. The catalytic residues of proteasome $\beta5i^{G201V}$ and β5i subunits. Thr73 is the most important catalytic residue within the N terminus of mature β5i. Only the amino acid side chains are shown. Nitrogen and oxygen atoms are blue and red, respectively. The G201V structure is shown in orange and the wild type is shown in green.

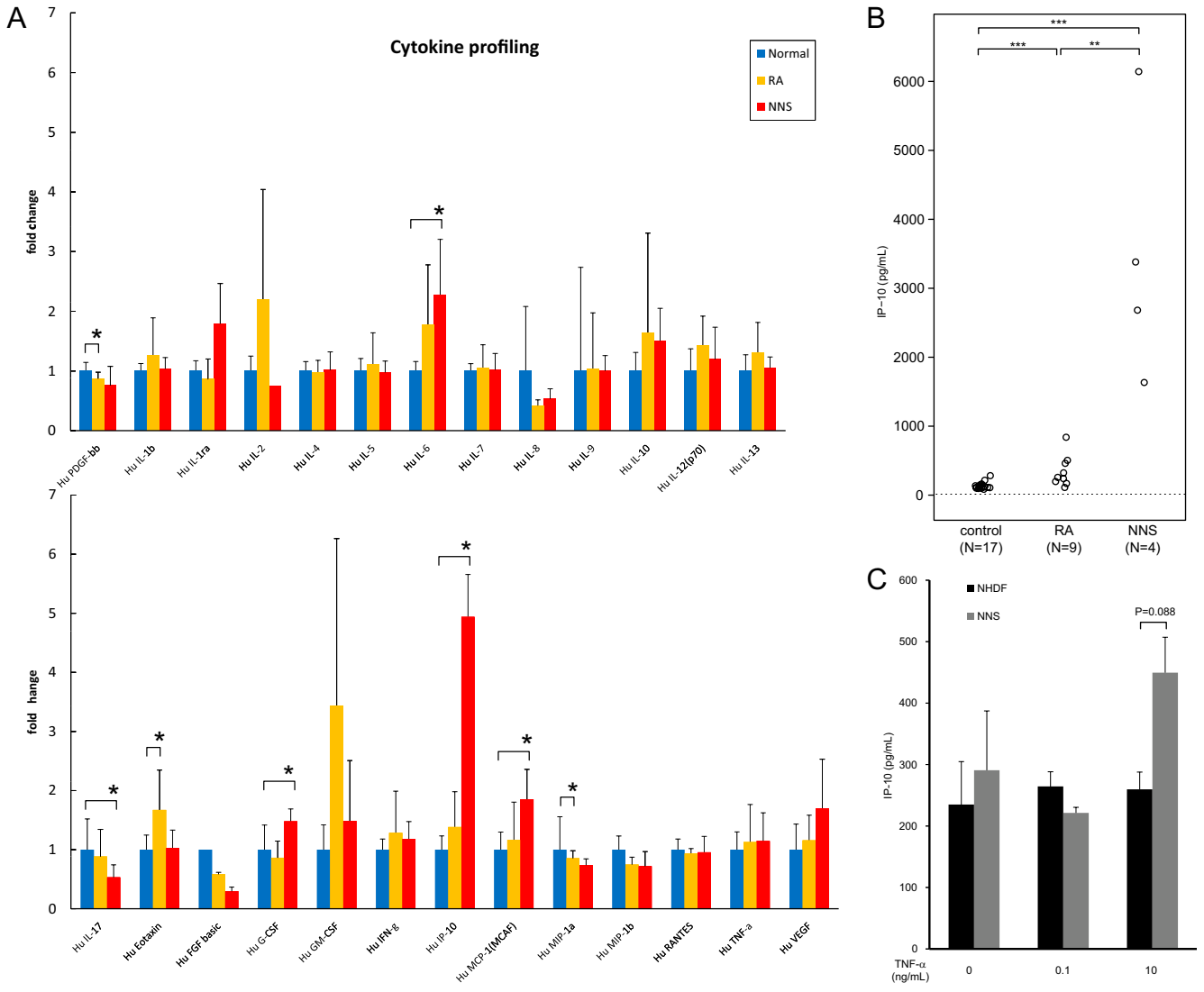

Fig. S3. Cytokine profiles in sera and conditional media from cultured fibroblasts. (*A*) Serum samples were obtained from healthy controls (n = 16), rheumatoid arthritis patients (RA; n = 10), and NNS patients (n = 4). The concentrations of 27 different cytokines were determined using a multiplex bead-based ELISA on a suspension array. Error bars indicate SD of the mean. P values were calculated using two-tailed Welch's t test. *$P \leq 0.05$. (*B*) IP-10 concentration in sera from patients with NNS and RA. IP-10 levels in sera were determined by ELISA on a suspension array. **$P \leq 0.01$, ***$P \leq 0.001$; Mann-Whitney u test. (*C*) IP-10 production by cultured fibroblasts. The concentrations of IP-10 in conditioned media were determined by ELISA (R&D Systems) using triplicate measurements. P, two-tailed Welch's t test.

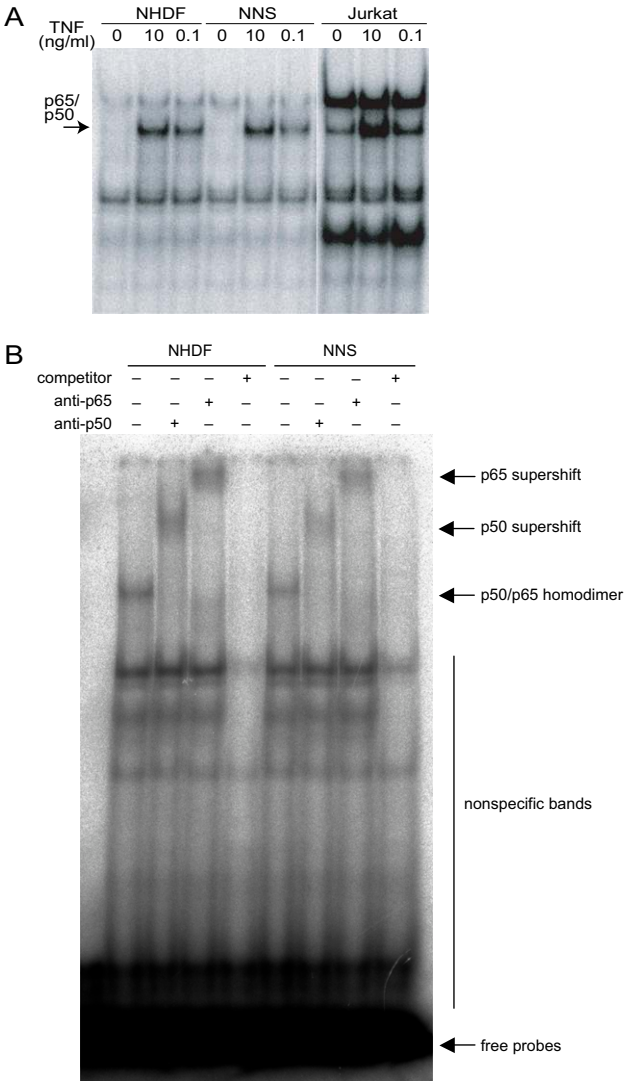

Fig. S4. NF-κB activity in fibroblasts from a NNS patient. (*A*) EMSA for NF-κB. EMSA with an NF-κB consensus probe was performed using nuclear extracts from normal human dermal fibroblast (NHDF), NNS fibroblasts, and Jurkat cells. The NF-κB signal was activated by TNF-α (10 ng/mL or 0.1 ng/mL) in all cell lines. (*B*) EMSA, using a specific antibody, was performed on nuclear extracts from NHDF and NNS after stimulation with TNF-α (10 ng/mL). The signal derived from the p50/p65 heterodimer was confirmed as a supershifted signal in both p50 and p65.

Table S1. Clinical features of our NNS patients compared to JMP syndrome

Patient	1	2	3	4	5	6	7	JMP (3 cases)
Present age, y (at death)	(47)	37	38	31	35	33	32	26–35
Sex	M	M	M	F	M	M	M	M/F
Parental consanguinity	+	+	–	+	–	–	–	–
Family history	+	–	–	–	–	–	–	±
Age at onset of pernio-like rash	–	2 mo	3 mo	6 mo	2 y	1 y	Infancy	–
Heliotrope-like periorbital rash	–	–	+	+	+	+	–	–
Nodular erythema-like eruptions	+	+	+	+	+	+	+	+
Age at onset of fever	12 y	Infancy	7 y	11 mo	2 y	2 y 4 mo	–	–
Partial lipomuscular atrophy	++	+	+	+	+	++	+	+
Long clubbed fingers	+	+	+	+	+	+	+	+
Joint contractures	++	–	+	+	+	++	+	++
Hyperhidrosis	–	+	+	++	–	–	+	NA
Short stature	–	–	–	–	–	+	–	+
Seizures	–	–	–	–	–	–	–	+
Low IQ	+	–	–	–	–	–	–	–
Microcytic anemia	–	+	+	+	+	+	+	+
Elevated ESR/CRP	+	+	+	+	+	+	+	+
High serum CPK	–	+	+	+	–	+	–	+
Hyper-γ-globulinemia	+	+	+	++	+	+	+	+
Antinuclear antibody titer	<40	<40	160	640	80	40	40	–
Positive autoantibody	–	–	MPO-ANCA	dsDNA	SS-A	dsDNA	–	–
Diabetes	+	–	–	–	–	–	–	–
Hypertriglyceridemia	–	–	–	+	+	+	+	–
Low HDL cholesterol	NA	+	–	+	+	+	+	+
Hepatosplenomegaly	+	NA	+	+	+	+	NA	+
Basal ganglia calcification	–	+	+	+	+	+	+	+
Reference	1, 2	3		4				5

All NNS patients have a c.602G > T mutation. M, male; F, female; y, years; mo, months; NA, not assessed; MPO, myeloperoxidase; ANCA, antineutrophil cytoplasmic antibody; ds, double stranded; JMP, joint contracture, muscular atrophy, microcytic anemia, and panniculitis-induced lipodystrophy.

1. Tanaka M, et al. (1993) Hereditary lipo-muscular atrophy with joint contracture, skin eruptions and hyper-gamma-globulinemia: A new syndrome. *Intern Med* 32:42–45.
2. Oyanagi K, et al. (1987) An autopsy case of a syndrome with muscular atrophy, decreased subcutaneous fat, skin eruption and hyper gamma-globulinemia: Peculiar vascular changes and muscle fiber degeneration. *Acta Neuropathol* 73:313–319.
3. Muramatsu T, Sakamoto K (1987) Secondary hypertrophic osteoperiostosis with pernio (Nakajo). *Skin Res* 29:727–731.
4. Kasagi S, et al. (2008) A case of periodic-fever-syndrome-like disorder with lipodystrophy, myositis, and autoimmune abnormalities. *Mod Rheumatol* 18:203–207.
5. Garg A, et al. (2010) An autosomal recessive syndrome of joint contracture, muscular atrophy, microcytic anemia, and panniculitis-associated lipodystrophy. *J Clin Endocrinol Metab* 95: E48–E63.